

Suppression of classical stochasticity by quantum-mechanical effects in the dynamics of periodically perturbed surface-state electrons

R. Blümel* and U. Smilansky

Department of Nuclear Physics, Weizmann Institute of Science, Rehovot 76100, Israel

(Received 11 January 1984)

We present the classical and the quantum-mechanical descriptions of surface-state electrons which are perturbed by a periodic force $F(t) = e\epsilon \sum_n \delta(t - T)$. The numerical results are supported by analytical estimates which indicate that the stochastic behavior which characterizes the classical treatment, and which is manifested by the energy diffusion and ionization rates, is suppressed in the quantum-mechanical treatment.

I. INTRODUCTION

The quantum-mechanical description of classically chaotic systems is a subject which has attracted much attention recently. In particular, the study of certain periodically perturbed one-dimensional systems (e.g., the kicked quantum rotor) demonstrate both analytically and numerically that classical stochasticity is suppressed in the quantum-mechanical description.¹⁻⁵ These pioneering studies open two important questions.

(a) Is the quantum suppression of classical stochasticity a general feature and, if not, what are the conditions for its emergence?

(b) Can one construct a semiclassical approximation which bridges between the quantum description and its classical limit, and enables the understanding of the former in terms of the corresponding classical concepts?

In an attempt to shed more light on these problems, Jensen⁶ proposed to study experimentally the effect of an rf electric field on surface-state electrons (SSE). Jensen's investigations of the Newtonian dynamics showed that chaotic behavior can be triggered by the external field. Moreover, the system is accessible to experimentation with present-day techniques and it is microscopic so that the emergence of quantum effects can be subject to experimental tests. Before carrying on with the discussion, a short review of the SSE is in order.

Surface-state electrons are electrons which bind to a liquid-helium surface by the induced electrostatic polarization. Grimes⁷ and his collaborators studied these electrons under various conditions and showed that the effective binding potential depends exclusively on the vertical distance x . To a good approximation it takes the form $V_{\text{eff}}(x) = Ze^2/x$, where Ze is the induced image charge. Because of the exclusion principle the liquid-He surface acts as an infinite repulsive wall.

An important feature of the SSE is that the external field may impart sufficient energy so that the electrons might become unbounded and separate (ionize) from the surface. Jensen showed that the dependence of the ionization efficiency on the field strength gives a direct indication of the onset of stochasticity.

In the present paper we study both classically and quantum mechanically the behavior of periodically per-

turbed SSE. Instead of studying the effect of a monochromatic rf field on the SSE we perturb them by a sharp, periodic $\delta(t)$ field. This enables us to solve both the classical and the quantum-mechanical problems and interpret the corresponding numerical results in terms of simple analytical estimates.

This study is motivated not only because of its relevance to a realistic system. Till now, most of the available information concerning the quantal treatment of classically stochastic dynamics came from the discussion of periodically kicked systems which are sufficiently different from the SSE to render its theoretical discussion interesting in its own right. (a) The spectrum of the unperturbed SSE has a continuum which is coupled to the discrete part of the spectrum by the periodic perturbation. To the best of our knowledge, the role of the continuum was never discussed in the present context. (b) The discrete spectrum of the SSE is of the type $E_n \approx -R/n^2$. Unlike the commonly studied systems with $E_n \propto n$ or $E_n \propto n^2$, the SSE spectrum has an accumulation point when $n \rightarrow \infty$, and the frequencies $(E_n - E_{n-1})/\hbar$ do not degenerate to one basic frequency and its harmonics. (c) The perturbation we apply corresponds to a spatially linear potential (constant field perpendicular to the liquid-He surface). The matrix elements in the SSE case increase as n^2 while in the standard cases the interaction is bounded.

The main goal of the present paper is to present a detailed comparison between the classical and the quantal description of the periodically perturbed SSE. Special emphasis will be given to those features which manifest or probe the classical stochasticity such as the diffusive nature of the energy gain and the ionization process.⁸

In Sec. II we shall describe the model Hamiltonian which will be solved classically in Sec. III and quantum mechanically in Sec. IV. The comparison between the two pictures and the summary will be given in Sec. V.

II. THE MODEL

As was mentioned in the Introduction, the SSE are adequately described in terms of an approximate Hamiltonian

$$H_0 = \frac{P^2}{2m} - \frac{Ze^2}{x}, \quad x > 0 \quad (2.1)$$

where x is the vertical distance from the wall and P is the conjugate momentum. It is supplemented with a perfect-elastic-reflection condition at $x=0$. We perturb the SSE by a periodic electric field which adds to the Hamiltonian a term

$$V(x,t) = -e\epsilon x \sum_k \delta(t - kT). \quad (2.2)$$

It is convenient to introduce the dimensionless Cartesian coordinate q and momentum p ,

$$q = \alpha x / 2, \quad p = 2P / \hbar \alpha, \quad (2.3)$$

where $\alpha = 2mZe^2 / \hbar^2$. The Hamiltonian becomes

$$H = H_0 + V(q,t) \\ = R \left[(p^2 - 2/q) - \beta q \sum_k \delta(t - \tau k) \right], \quad (2.4)$$

where we introduced the effective Rydberg constant

$$R = m (Ze^2)^2 / 2\hbar^2 = \hbar^2 \alpha^2 / 8m$$

and

$$\beta = 2e\epsilon / \hbar \alpha.$$

Time is measured in units of \hbar/R , and $\tau = TR / \hbar$.

Between kicks it is more appropriate to discuss the evolution in terms of the action angle variables (n, θ) . The canonical transformation which defines (n, θ) in terms of (p, q) is

$$n = \left[\frac{2}{q} - p^2 \right]^{-1/2}, \quad (2.5a)$$

$$\theta = F(\eta) = \begin{cases} 2[\eta - \frac{1}{2} \sin(2\eta)], & p \geq 0 \\ 2\pi - 2[\eta - \frac{1}{2} \sin(2\eta)], & p < 0 \end{cases} \quad (2.5b)$$

where

$$\eta = \arcsin(q/2n^2)^{1/2}.$$

One can easily check that the Jacobian matrix

$$\frac{\partial(p,q)}{\partial(n,\theta)} = \begin{bmatrix} -p/n & -n^3/q^2 \\ 2q/n & n^3 p \end{bmatrix}, \quad (2.6)$$

$$\det \left[\frac{\partial(p,q)}{\partial(n,\theta)} \right] = n^2 \left[\frac{2}{q} - p^2 \right] = 1.$$

It should be pointed out that the above relations are valid only for the bounded motion, $H_0 < 0$. In the (n, θ) representation

$$H = R \left[-1/n^2 - 2\beta n^2 \sin^2 \eta \sum_k \delta(t - k\tau) \right] \quad (2.7)$$

and η is obtained from θ by inverting equation (2.5b).

The system is completely defined once the initial conditions are specified. For the quantum-mechanical treatment we shall assume that the initial wave function is an eigenstate of H_0 with a principal quantum number n_0 ,

$$H_0 |n_0\rangle = -(R/n_0^2) |n_0\rangle. \quad (2.8)$$

The classical analog is a phase-space distribution function

$$\sigma(n, \theta) = (1/2\pi) \delta(n - n_0). \quad (2.9)$$

In the following sections we shall discuss separately the classical and the quantum-mechanical equations of motion and compare their predictions about the evolution of the perturbed SSE system.

III. CLASSICAL DYNAMICS

The classical equations of motion derived from the model Hamiltonian discussed in Sec. II define a discrete, area-preserving mapping of phase space onto itself. Denoting by (n_k, θ_k) the phase-space point just before the k th kick, we shall present the mapping which gives (n_{k+1}, θ_{k+1}) in terms of (n_k, θ_k) .

The potential term in (2.7) depends on both θ and n . Since n is discontinuous at the kick, it is difficult to construct the dynamical mapping based on this form of the Hamiltonian. This problem can be naturally solved by canonically transforming to the Cartesian (p, q) representation where the potential is linear in q and is independent of p . Thus the map will be constituted of a few steps in which canonical transformations are interwoven with dynamical mappings.

Step 1. Canonical transformation from (n_k, θ_k) to (p_k, q_k) :

$$p_k = \frac{1}{n_k} \cot(\eta_k), \\ q_k = 2n_k^2 \sin^2(\eta_k), \\ \eta_k = F^{-1}(\theta_k), \quad (3.1)$$

and F^{-1} is the inverse of F defined in (2.5).

Step 2. The equations of motion in the (p, q) representation yield the phase-space point just after the kick $(\tilde{p}_k, \tilde{q}_k)$:

$$\tilde{p}_k = p_k + \beta, \\ \tilde{q}_k = q_k, \\ \tilde{E}_k = \tilde{p}_k^2 - 2/\tilde{q}_k = E_k + 2p_k\beta + \beta^2, \quad (3.2)$$

where E is the energy in units of R .

Step 3. Canonical transformation of $(\tilde{p}_k, \tilde{q}_k)$ to $(\tilde{n}_k, \tilde{\theta}_k)$:

$$\tilde{n}_k = (2/\tilde{q}_k - \tilde{p}_k^2)^{-1/2} = (-\tilde{E}_k)^{-1/2}, \\ \tilde{\theta}_k = F(\tilde{\eta}_k), \quad (3.3)$$

where

$$\tilde{\eta}_k = \arcsin(\tilde{q}_k/2\tilde{n}_k^2)^{1/2}.$$

Step 4. Free propagation between the kicks:

$$n_{k+1} = \tilde{n}_k, \\ \theta_{k+1} = [\tilde{\theta}_k + \omega(\tilde{n}_k)\tau] \pmod{2\pi} \\ \omega(n) = \frac{1}{R} \frac{\partial H_0}{\partial n} = 2/n^3. \quad (3.4)$$

This completes the definition of the classical mapping. Since each of the four steps is area preserving, so is their product, and

$$\det \left[\frac{\partial(n_{k+1}, \theta_{k+1})}{\partial(n_k, \theta_k)} \right] = 1.$$

The classical mapping can be repeated as long as the trajectory remains bounded, with $\bar{E}_k < 0$ in step 2 [Eq. (3.2)]. Positive energies can be reached if (a) the energy E is so close to the ionization threshold that the mean energy gain per step β^2 exceeds $|E_k|$. Since the momentum p can point at either direction with the same probability, ionization will occur with a 50% chance. (b) Because of the singular nature of the potential, when $q \rightarrow 0$, p diverges like $q^{-1/2}$ so that the term $2p_k\beta$ may become large and positive. For $\beta \ll 1/n$, this will happen when $q/2n^2 < 4(\beta n)^2$ or, in terms of the angle variable, $\theta \leq 32/3(\beta n)^3$. Thus, if the initial n value satisfies

$$n_0\beta \ll 1 \quad (3.5)$$

the direct ionization mechanism, discussed under (b) above, becomes very unlikely and the bounded motion can be studied during a long time interval. Eventually, a large value of n_k will be reached so that ionization may occur with higher probability. Under these conditions the ionization can serve as a probe to study the bounded motion.

The classical description of the SSE dynamics is obtained by applying the mapping discussed above to an ensemble of phase-space points which is initially given by (2.9). Whenever a trajectory ionizes, it is removed from the ensemble.

In most of the numerical studies we chose $n_0 = 10$ or thereabouts. This choice was made because of our special interest in the semiclassical regime where the quantum numbers are large and the correspondence between the quantum and the classical pictures is expected to be clearer. This choice of n_0 dictates the range of variations for the other parameters. β must be of the order of 10^{-3} so that (3.5) is satisfied. In order to study the onset of stochasticity we must have $\omega(n_0)\tau \geq 2\pi$ hence $\tau \sim 10^3$. Typically 100–500 phase-space points (trajectories) were used to represent the classical distribution function. Statistical errors of the order of 7% are therefore expected in any quantity which is calculated as an ensemble average. The following properties characterize the classical dynamics.

A. The stability matrix and the Lyapunov exponent

The one-step stability matrix $\partial(n_{k+1}, \theta_{k+1})/\partial(n_k, \theta_k)$ (Jacobian) is constructed by following the steps 1–4. Its determinant is unity and its trace can be written as

$$\begin{aligned} S &= \text{Tr} \left[\frac{\partial(n_{k+1}, \theta_{k+1})}{\partial(n_k, \theta_k)} \right], \\ &= \frac{1}{2\nu} \left[\nu^2 + \frac{1}{\nu^2} \right] (1 + \nu^2 + n_k^2\beta^2) + \frac{6\tau}{q_k^2} n_k^2\beta\nu, \end{aligned} \quad (3.6)$$

where $\nu = n_k/n_{k+1}$ and $q_k = q(n_k, \theta_k)$. As long as

$|S| \leq 2$, the eigenvalues of the stability matrix are unimodular, which implies that the trajectory is locally regular. When $|S| > 2$, one of the eigenvalues, λ_+ , exceeds 1 in absolute magnitude and the trajectory is locally unstable. The local Lyapunov exponent is defined as

$$L_p(n_k, \theta_k) = \ln |\lambda_+(n_k, \theta_k)|. \quad (3.7)$$

For systems with $\beta > 0$ (the field pushes the electron away from the He surface), the expression (3.6) for S is larger than 2 for all values of the parameters. Thus the local Lyapunov exponent is always positive which implies that the classical motion of the SSE subject to such a periodic field is always mixing. A typical trajectory is shown in Fig. 1(a), where the points in the (n, θ) plane represent values assumed by a single trajectory. Once the trajectory reaches higher values of n , the motion becomes less and less chaotic. Ionization finally takes place after a succession of steps, which on the scale of the plot seem to be completely regular. This can be explained by recalling that the chaotic nature of the mapping is due to the “stretching and folding” mechanism which is embodied in

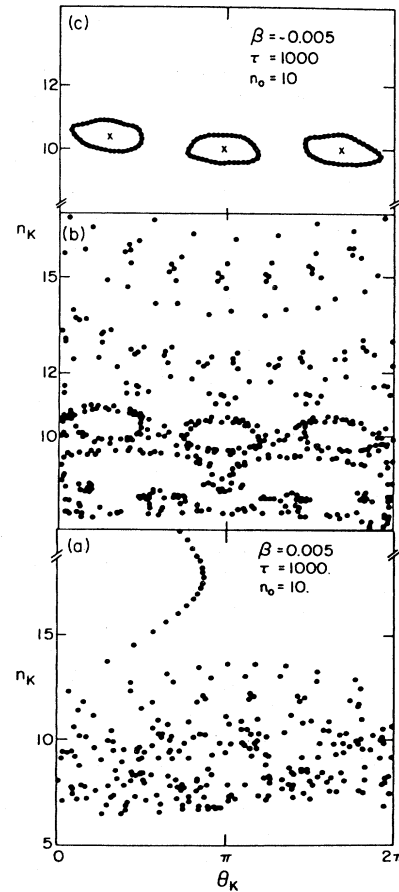


FIG. 1. Classical trajectories (a) $\beta = +0.005$ chaotic trajectory leading to ionization; (b) $\beta = -0.005$, chaotic trajectory; (c) $\beta = -0.005$, stable periodic trajectory. A fix point (period three) of the classical mapping is marked by \times .

Eq. (3.4). Its effectiveness decreases rapidly as n increases. An alternative viewpoint can be obtained by considering the dependence of λ_+ on n and θ . As long as $n_k < 1/\beta$, and for almost all values of θ_k ,

$$\lambda_+ \cong 1 + \frac{n_k}{q_k} (6\tau\beta)^{1/2}.$$

Hence

$$\langle L_p \rangle \cong (6\tau\beta \langle n^{-2} \rangle)^{1/2}, \quad (3.8)$$

where the angular brackets denote an ensemble average. The mean Lyapunov exponent approaches zero as n increases, which is responsible for the apparently regular motion of the system for large n values.

In Fig. 2(a) we show the distribution of $\lambda_+(n_k, \theta_k)$ values for a given trajectory. λ_+ is largest near the points $\theta=0, 2\pi$ which reflect the singular behavior of the Coulomb potential. Note that λ_+ always exceeds the value 1. The relation (3.8) was confirmed numerically as shown in Fig. 3.

The situation is quite different when $\beta < 0$ (the field pushes the electron *towards* the liquid-He surface). Here, for any given value of the parameters β and τ , phase space is divided into two distinct regions. One region corresponds to positive local Lyapunov exponents where the motion is locally mixing. This region extends over the entire θ range for $n < (3\tau|\beta|/8)^{1/2}$. [This estimate is derived by checking when the point $(n, \theta=\pi)$ becomes locally unstable.] For larger n values the stochastic region reduces to strips near $\theta=0, 2\pi$, which become narrower with increasing n . In the complementary region, the

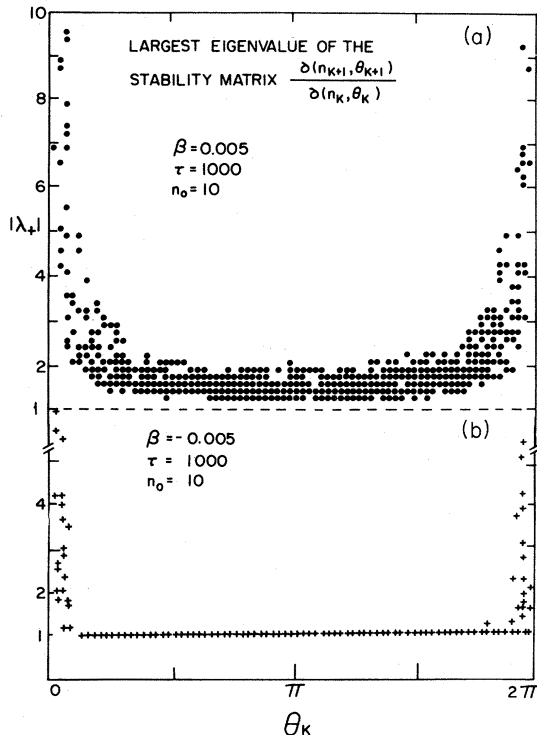


FIG. 2. Distribution of $\lambda_+(n_k, \theta_k)$ for two typical chaotic trajectories. (a) $\beta > 0$, (b) $\beta < 0$.

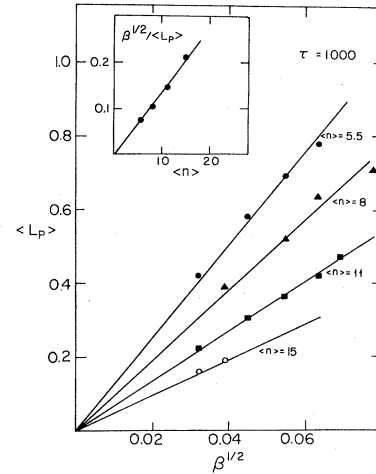


FIG. 3. Dependence of the mean Lyapunov exponent on $\langle n \rangle$ and β , checking the estimate (3.8).

motion is stable with $|\lambda_+(n, \theta)| = 1$. Two typical trajectories with $\beta < 0$ are shown in Figs. 1(b) and 1(c). Figure 1(c) displays a stable periodic orbit. It is confined to the region where $|\lambda_+(n, \theta)| = 1$. Figure 1(b) presents a stochastic trajectory which differs from the previous trajectory by a slight shift in the initial value. The diffusion of points is not strong enough to mask the underlying regular patterns. The distribution of λ_+ values corresponding to the latter trajectory is displayed in Fig. 2(b). The slight overlap of this trajectory with the region in phase space where $\lambda_+ > 1$ introduces the stochastic nature of this orbit.

We have also calculated the N step stability matrix $\partial(n_N, \theta_N)/\partial(n_0, \theta_0)$ and evaluated the ensemble-averaged value of its larger eigenvalue. This did not differ significantly from the product of the local $\langle \lambda_+ \rangle$ values.

The distribution of λ_+ values within the ensemble was studied. For cases with $\beta > 0$ the distribution is quite narrow and peaks around the mean value. For $\beta < 0$, two peaks usually occur—one corresponds to the regular trajectories with $|\lambda_+| = 1$, while the other comes from the stochastic trajectories and is similar to the peak observed for $\beta > 0$.

B. Energy diffusion

One of the features which characterize the onset of stochasticity in periodically perturbed systems is that the energy gain is diffusive, that is, the second moment of the energy distribution increases linearly with time. In the present case

$$\begin{aligned} \langle E_N \rangle &= E_0 + N\beta^2 = -n_0^{-2} + N\beta^2, \\ (\Delta E)^2 &\equiv \langle (E_N^2 - \langle E_N \rangle^2) \rangle \\ &= 4\beta^2 \left\langle \sum_{k=0}^{N-1} (p_k)^2 \right\rangle \cong 4\beta^2 \langle n^{-2} \rangle N \end{aligned} \quad (3.9)$$

which can be easily obtained from (3.2) by assuming $\langle p_k \rangle = 0$ and $\langle p_k p_l \rangle = \delta_{kl} \langle n^{-2} \rangle$. These relations are expected for stochastic systems and should be satisfied

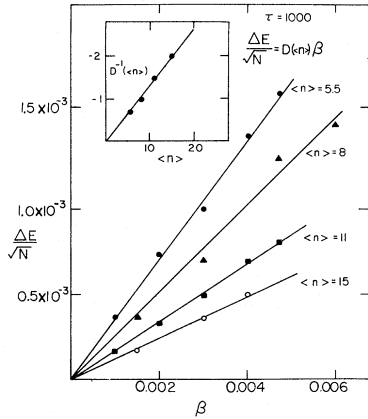


FIG. 4. Dependence of the diffusion coefficient for the energy distribution on β and $\langle n \rangle$, checking the estimate (3.9).

whenever $\beta > 0$. The relation (3.9) was tested numerically under various conditions. The linear dependence of the second moment on N is well reproduced over large time intervals (for $\beta \sim 10^{-3}$, $n_0 = 10$, and $\tau \sim 10^3$, typical values for N range from 10^3 to 10^4). Averaging over statistical fluctuations, we check the dependence of the diffusion coefficient $\Delta E/\sqrt{N}$ on β and $\langle n^{-2} \rangle$. The good agreement between the numerical results and the estimate (3.9) is displayed in Fig. 4. Note that the expression (3.9) is independent of τ . We checked this numerically by varying τ between $\tau = 500$ and 10000 . The diffusion coefficient is indeed independent of τ within the statistical error. When $\tau = 100$ or less the mixing properties are too weak to manifest themselves within 1000 kicks, and on this time scale the assumptions which underlie the derivation of (3.9) are not valid. Calculating higher moments of the energy distribution we found that the energy distribution is not Gaussian.

As was explained in the preceding section, systems with $\beta < 0$ accommodate both periodic and stochastic trajectories. The former do not gain energy on the average and therefore the details of the energy distribution depend strongly on the relative weight of the two types of trajectories in the ensemble.

C. Ionization rates

As was discussed above, we consider a trajectory as being ionized and removed from the phase-point ensemble once its energy becomes positive. Owing to the long-range nature of the binding Coulomb potential and the constancy of the force in space, an electron with positive energy may be trapped back. This is quite unlikely, especially when $\beta > 0$ so that the external field pushes the electron away from the He surface. Since most of the discussion of ionization rates will concentrate on systems with $\beta > 0$ we adopt the above definition of ionization.

In order to define the ionization rates, we consider the fraction of trajectories which remain bound after N kicks and denote it by $P_B(N)$. Some examples of this function are shown in Fig. 5. The depletion due to ionization is not quite exponential but the mean ionization rate can be

characterized by

$$I_R = -\frac{1}{P_B(N)} \frac{dP_B(N)}{dN}. \quad (3.10)$$

Calculated at the point where $P_B(N)$ assumes a certain prescribed value, e.g., when $P_B(N) = \frac{1}{2}$. We shall estimate I_R in two ways which differ in the mechanism assumed to induce the ionization process.

(i) *Diffusive ionization.* The stochastic nature of the system implies that energy is gained via a diffusive process so that the energy distribution after the N th kick may be approximated as

$$f(E, N) = \frac{1}{\Delta E(N)} g([E - \langle E(N) \rangle] / \Delta E(N)), \quad (3.11)$$

where $\Delta E(N)$ is defined in (3.9), and $g(x)$ is yet an unspecified function normalized by requiring $\int g(x) dx = 1$. We approximate $P_B(N)$ by

$$P_B(N) = \int_{-\infty}^0 dE f(E, N) = \int_{-\infty}^{-\langle E(N) \rangle / \Delta E(N)} dx g(x).$$

Using this expression in (3.10), at the point where $P_B(N) = \frac{1}{2}$ and to lowest order in β , we obtain

$$I_R \approx K \beta^2 / \langle E \rangle = K \beta^2 / \langle n^{-2} \rangle, \quad (3.12)$$

where the proportionality coefficient K depends on the detailed form of $g(x)$.

(ii) *Direct ionization.* We have shown above that the singular nature of the binding Coulomb potential is responsible for direct ionization for any SSE whose distance from the liquid surface is less than $q_{\text{ion}} = 8n^2(\beta n)^2$. This value of q can be also expressed in terms of a limiting angle θ_{ion} . If the system displays stochastic features, the angle θ is evenly distributed on the interval $[0, 2\pi]$ and, therefore, the ionization probability per step will read

$$I_R = \theta_{\text{ion}} / 2\pi \approx (32/6\pi) \beta^3 \langle n^3 \rangle. \quad (3.13)$$

We see that the two mechanisms predict a different dependence of I_R on β .

Our numerical investigations support the assumption that ionization is due to a diffusive energy gain. This is demonstrated in the inset in Fig. 5. The fact that the diffusion coefficient is independent of τ is responsible for the observation that I_R are also independent of τ .

When $\beta < 0$, the stable periodic orbits never ionize, whereas the stochastic trajectories follow much the same route to ionization as discussed for the $\beta > 0$ case. We find that the probability of the SSE to remain bound in the limit of large N is equal to the fraction of periodic orbits in the ensemble.⁹

The classical description of the SSE system can be summarized in the following way. Whenever the condition (3.5) is fulfilled, the "lifetime" of the bound SSE against ionization is very large [of the order of $(n_0\beta)^{-2}$], and the ionization process can be used to probe the mechanism with which energy is transmitted to the SSE. The simple analytical estimates which are supported by detailed numerical studies show that, within the life span of the system, the stochastic features dominate. This was established by considering the Lyapunov exponent, the energy dis-

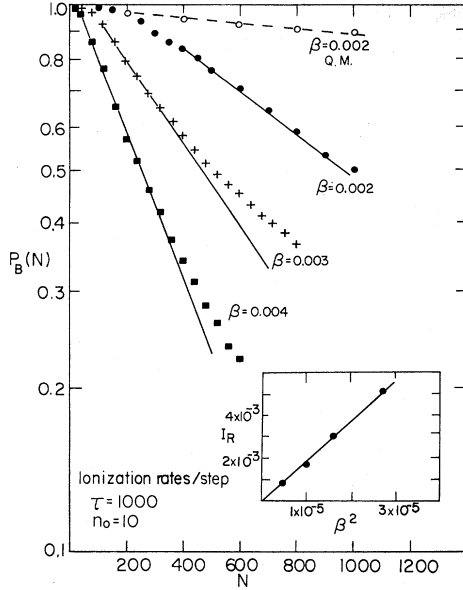


FIG. 5. Probability to remain bound $P_B(N)$ for various values of β . Inset checks the classical result (4.12). A quantum mechanical $P_B(N)$ is denoted by the letters QM.

tribution, and, finally, the ionization rates.

We have also shown that the stochastic features of the system are less apparent when the mean energy increases. This behavior contrasts with that observed for other periodically perturbed systems such as, e.g., the periodically kicked rotor.

IV. QUANTUM MECHANICS

The quantum-mechanical analog of the classical Hamiltonian is obtained by a straightforward quantization of H_0 and $V(x,t)$ of Eqs. (2.1) and (2.2). The eigenstates of H_0 and the corresponding spectrum are determined by the boundary condition that the wave function must vanish at $x=0$. The bound states are completely specified by the principal quantum number n , which is the quantum analog of the classical action variable defined in Sec. II. The continuum states are specified by the wave number χ . The corresponding wave functions are

$$\begin{aligned} \langle x | n \rangle &\equiv \psi_n(x) \\ &= \left[\frac{\alpha}{2n^3} \right]^{1/2} \left[\frac{\alpha x}{n} \right] L_{n-1}^{(1)} \left[\frac{\alpha x}{n} \right] \\ &\quad \times \exp \left[-\frac{\alpha x}{2n} \right], \quad n = 1, 2, \dots \end{aligned} \quad (4.1)$$

$$E_N = -R/n^2,$$

$$\langle x | \chi \rangle \equiv \psi_\chi(x) = \left[\frac{2}{\pi} \right]^{1/2} F_0(\eta, \chi x), \quad (4.2)$$

$$E_\chi = \frac{\hbar^2}{2m} \chi^2,$$

where $L_n^{(1)}$ is the Laguerre polynomial and $F_0(\eta, \chi x)$ is

the regular Coulomb function and $\eta = -\alpha/2\chi$. The normalization is chosen such that

$$\langle n | n' \rangle = \delta_{nn'}, \quad \langle \chi | \chi' \rangle = \delta(\chi - \chi'), \quad \langle n | \chi \rangle = 0. \quad (4.3)$$

The quantum-mechanical propagation of the SSE under the periodic potential can be easily expressed as a discrete norm-preserving mapping of the Hilbert space onto itself. Denoting by $|\Psi_k\rangle$ the wave function just before the k th kick, it is related to $|\Psi_{k+1}\rangle$ by

$$|\Psi_{k+1}\rangle = e^{-i\tau H_0} e^{-iV(x)} |\Psi_k\rangle = e^{-iW} |\Psi_k\rangle. \quad (4.4)$$

As before, H_0 is the Hamiltonian (2.1) measured in units of R and $V(x) = -\beta\alpha x/2$. Equation (4.4) defines the Hermitian operator W in terms of which the one-step propagator will be discussed in the sequel.

In line with the classical description, we shall consider only such cases where ionization is weak enough to consider it a small perturbation of the bounded motion. This allows us to develop the quantum picture by successive approximations which differ as a result of the order in which the effects of the continuum are considered.

A. Complete exclusion of continuum effects

The description of the bounded motion is obtained by replacing the mapping (4.4) by

$$|\Psi_{k+1}\rangle = e^{-i\tau H_0} e^{-iPV(x)P} |\Psi_k\rangle, \quad (4.5)$$

where $P = \sum_n |n\rangle\langle n|$ is the projector on the subspace spanned by the bound states of H_0 . Since PVP is a Hermitian operator the mapping (4.5) is norm preserving.

Analytical expressions for the matrix elements of V are given in the Appendix. In practice, the basis set is truncated and the finite matrix V is numerically exponentiated. Typically, we included approximately 100 states in the basis. In all cases the basis set was large enough to guarantee that the results are insensitive to a further increase in its size.

In almost all the calculations reported here we chose the initial state to be the $n_0 = 10$ state. This was motivated by our interest in the correspondence between the classical and the quantum pictures which is expected to become more apparent when the quantum numbers are large.

Iterating the map (4.5) we calculated the expectation values of H_0 and H_0^2 as a function of the kick number N for various values of the parameters β , τ , and n_0 . In contrast with the classical results, the second moment of the energy distribution remains bounded. The rate of the initial increase of the width, as well as the maximum value reached, are very sensitive to the strength and the period of the external force.

Similar suppression of the energy diffusion was observed in the quantum-mechanical treatment of the periodically kicked rotor.^{4,5} In the latter case the quantum results were explained by showing the formal similarity between the rotor problem and the Anderson localization in one dimension. For the periodically kicked SSE

the analogous Anderson problem does not correspond to any physically interesting solid-state problem and therefore was never studied. In spite of this, the theoretical tools which were devised to study the quantum rotor will be used below for the interpretation of the SSE results.

The natural framework for the discussion of the quantum mapping is the quasienergy representation. In the present case this can be introduced by considering the eigenstates $|\alpha\rangle$ and the corresponding eigenvalues ω_α of the Hermitian operator W defined in Eq. (4.4). It can be easily shown that

$$|\Psi_N\rangle = \sum_{\alpha} e^{-i\omega_{\alpha}N} \langle \alpha | n_0 \rangle |\alpha\rangle \quad (4.6)$$

and therefore the wave function is completely determined by the expansion coefficients $\langle \alpha | n_0 \rangle$. Moreover, the probability amplitudes

$$P_{\alpha}(n_0) = |\langle \alpha | \Psi_N \rangle|^2 = |\langle \alpha | n_0 \rangle|^2 \quad (4.7)$$

are independent of N and represent the distribution of the initial state $|n_0\rangle$ among the quasienergy eigenstates.

Following Grempel *et al.*,⁵ we explain the calculated behavior of the quantum-mechanical energy distribution by examining the degree of localization of the expansion coefficients $\langle \alpha | n_0 \rangle$. When only a few quasienergy states take part in the development of the wave function $|\Psi_N\rangle$, all observables will be bound since $\langle n | \Psi_N \rangle$ will be quasi-periodic.

A convenient measure for the degree of localization is the width function

$$\Delta(n_0) = \exp \left[- \sum_{\alpha} P_{\alpha}(n_0) \ln P_{\alpha}(n_0) \right]. \quad (4.8)$$

This function tends to unity if the $P_{\alpha}(n_0)$ are completely localized on one state, and it takes the value A if the $P_{\alpha}(n_0)$ are uniformly distributed over A states. The width function is displayed in Fig. 6 for a few values of the parameters (β, τ) . At low n_0 values $\Delta(n_0) \cong 1$ which implies that $|n_0\rangle$ is localized on one eigenstate of W . An abrupt change in the localization patterns occurs at some $n_0 = n_{\text{crit}}(\beta, \tau)$, beyond which $\Delta(n_0)$ increases rapidly till it approaches the width function which was calcu-

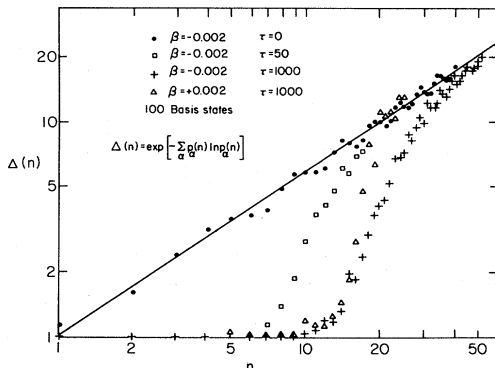


FIG. 6. Width function $\Delta(n)$ for various values of β and τ . Line through the $\tau=0$ points is drawn to guide the eye.

lated for $\tau=0$ where $W=V$. This is the maximal spread which V can induce and in the present case it is not sufficient to bring about a complete delocalization. Studying a large number of cases we observed that the dependence of n_{crit} on β and τ can be well reproduced by

$$n_{\text{crit}} = \text{const} \times (\tau/\beta)^{1/5}. \quad (4.9)$$

We shall explain this behavior below. In order to demonstrate the relation between the width function $\Delta(n)$ and the properties of the calculated wave function, we calculated

$$\sigma_N(n) = (\langle \Psi_N | n^2 | \Psi_N \rangle - \langle \Psi_N | n | \Psi_N \rangle^2)^{1/2}$$

and

$$P_N(n_0) = |\langle \Psi_N | n_0 \rangle|^2.$$

These functions exhibit complicated oscillations with N , and in Table I we quote their upper and lower bounds and show their variations as n_0 is scanned across the region where $\Delta(n_0)$ is changing rapidly. The calculations were carried out for $\beta=0.002$ and $\tau=1000$. The corresponding $\Delta(n_0)$ function is shown in Fig. 6 (triangles). Figure 7 displays the function $\sigma_N(n)$ for $n_0=8, 16, 20, 30$.

In order to get a better insight into the observed results we expand W to first order in V . This can be achieved by using the method of Ref. 10 and making use of the fact that H_0 is diagonal:

$$\langle n | W | m \rangle \cong \begin{cases} \langle n | V | m \rangle \frac{i(E_n - E_m)\tau}{1 - \exp[-i(E_n - E_m)\tau]}, & n \neq m \\ \tau E_n + \langle n | V | n \rangle, & n = m. \end{cases} \quad (4.10)$$

The eigenstates $|\alpha\rangle$ of W will certainly be well localized in the $|n\rangle$ representation if the perturbation expansion is justified, in other words, $\tau(E_n - E_{n+j}) > \langle n | V | n+j \rangle$. In the present case $E_n \sim -1/n^2$ and $\langle n | V | n+j \rangle \sim \beta n^2$ and the above condition reads $2\tau/n^3 > \text{const} \times \beta n^2$. This condition cannot be satisfied

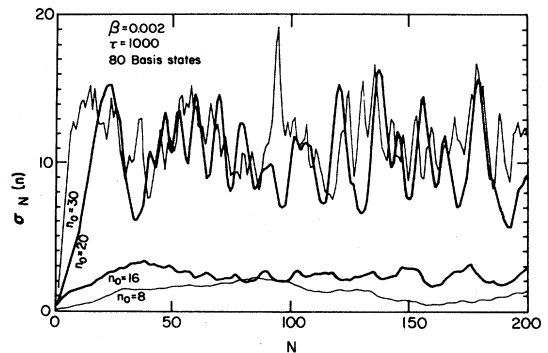


FIG. 7. RMS deviation of the n distribution as a function of the kick number N , for various initial conditions (norm-preserving quantal mapping).

simultaneously for all n values, and it breaks down for $n > \text{const} \times (\tau/\beta)^{1/5}$. This estimate agrees well with the observed behavior discussed in connection with Eq. (4.9).

The factor which appears in the first-order expression of the off-diagonal matrix elements of W can lead to resonant mixing of states for which $\tau(E_n - E_m) \cong 0 \pmod{2\pi}$. In such cases, the states $|n\rangle$ and $|m\rangle$ will have large overlaps with two eigenvectors of W , even though $n, m < n_{\text{crit}}$. These resonances cannot be avoided as long as $|\tau E_{n_0}| > 2\pi$, and their effect can be studied by approaching the resonance condition arbitrarily closely by changing τ . Near resonance the width of the energy distribution increases rapidly during the first few iterations of the map. The rate of change is strongly dependent on the proximity to the resonance. Beyond the transient stage the distributions exhibit the complicated but bounded oscillations which were discussed above. The effect of the resonant mixing on the ionization rates will be discussed below.

The most important result of the above discussion is that the localized nature of the wave function suppresses the stochastic features which characterized the classical dynamics. In this respect the present system is similar to the periodically kicked rotor, although the localization pattern for the SSE system reveals more structure. As will be shown in the following sections, the inclusion of the continuum does not alter the localized nature of the wave function as far as its bounded component is concerned.

B. Inclusion of continuum effects—lowest order

An approximation which takes into account the transitions to the continuum is obtained from the exact mapping (4.4) by approximating $|\Psi_N\rangle$ by $P|\Psi_N\rangle$, where P is the projector on the bounded subspace. The quantum mapping now reads

$$|P\Psi_{N+1}\rangle = e^{-iH_0\tau} P e^{-iV} P |\Psi_N\rangle \quad (4.11)$$

and the essential difference between (4.11) and (4.5) is that $P e^{-iV} P$ is not a unitary operator whereas $e^{-iV} P$ is unitary. The physical picture which underlies the mapping (4.11) is that transitions from the continuum back to the P space have a negligible effect on the further development of the projected wave function. A similar approximation was adopted for the classical calculations. In Sec. IV C we shall show that (4.11) is a lowest-order term in a consistent expansion of the exact quantum mapping.

The dissipation of probability from the projected wave

function did not alter appreciably the calculated distribution of energy. If anything, the variance of the n distribution became smaller, due to the more efficient ionization from higher- n components. Some representative results are shown in Table I.

The norm

$$P_B(N) = \langle \Psi_N | P \Psi_N \rangle \quad (4.12)$$

is the probability to remain bounded till the N th kick, and the ionization rate I_R can be defined in complete analogy to Eq. (3.10). A quantum mechanical $P_B(N)$ is plotted in Fig. 5 and its logarithmic derivative is almost constant over the entire range. [Note the large discrepancy between the classical and quantum-mechanical predictions for $P_B(N)$.]

To investigate the quantum description of the ionization process we present detailed studies of a few systems. In the first we fix $n_0 = 10$ and $\tau = 500$ and calculate $I_R(\beta)$ for $1 \times 10^{-3} < \beta < 3 \times 10^{-3}$. The results are plotted in Fig. 8 together with the corresponding classical values. The two sets differ by a factor of ~ 10 . To check the quantum results we evaluated the ionization rate from a pure bound state $|n_0\rangle$ by performing the integral

$$I_R^{(n_0)}(\beta) = \int_0^\infty d\chi | \langle n_0 | e^{-iV} | \chi \rangle |^2. \quad (4.13)$$

The matrix elements $\langle n | e^{-iV} | \chi \rangle$ can be evaluated analytically in terms of Jacobi polynomials and the expressions are quoted in the Appendix. Note that $I_R^{(n_0)}(\beta)$ is independent of τ and depends on the magnitude of β and *not* on its sign. The expression (4.13) is expected to give a good approximation in situations where the wave function $|\Psi_N\rangle$ is very well localized on one state $|n_0\rangle$. This is indeed the case here since for $\tau = 500$ and $\beta = 3 \times 10^{-3}$, $n_{\text{crit}} = 11.7$ [Eq. (4.9)]. Also, $\tau/n_0^2 = 5$ and therefore the state $|n_0 = 10\rangle$ cannot mix resonantly with any other state. The excellent agreement between the values of $I_R(\beta)$ and $I_R^{(n_0=10)}(\beta)$ and the fact that $I_R(\beta < 0)$ were found to be almost indistinguishable from $I_R(\beta > 0)$ can be considered as evidence, provided by the ionization process, of the fact that $|\Psi_N\rangle$ is localized.

The ionization rates for a system with $\tau = 1000$ are shown in Fig. 9, and here the situation is not that simple. For $|\beta| \lesssim 1.5 \times 10^{-3}$ the ionization rates agree quite nicely with the expression $I_R^{(n_0=10)}(\beta)$ and also $I_R(\beta) \cong I_R(-\beta)$. The classical ionization rates for $\tau = 1000$ are quite close to the ones calculated for $\tau = 500$, and the discrepancy of a factor of 10 between the classical and quantum-mechanical results also remains in this case.

TABLE I. Comparison of the n distributions obtained by the quantum mappings (4.5) and (4.11). Functions $\sigma_N(n)$ and $P(n_0)$ are defined in the text. Here, $\beta = 0.002$ and $\tau = 1000$.

n_0	$\Delta(n_0)$	Norm-preserving mapping [Eq. (4.5)]			Norm-dissipating mapping [Eq. (4.11)]		
		$\max[\sigma_N(n)]$	$\min[\sigma_N(n)]$	$\min P(n_0)$	$\max[\sigma_N(n)]$	$\min[\sigma_N(n)]$	$\min P(n_0)$
8	1.02	2.3	0.5	0.989	1.2	1.0	0.977
16	1.9	3.4	1.7	0.27	2.6	0.7	0.26
20	4.3	16.3	5.7	0.02	13.7	4.3	0.01
30	10	19.0	7.5	0.003	16.8	5.8	0.0001

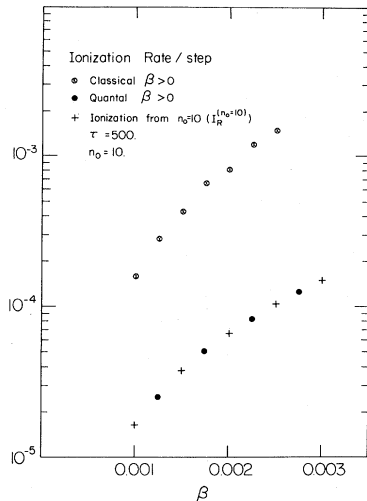


FIG. 8. Ionization rates calculated in various approaches for $\tau=500$.

For $|\beta| > 1.5 \times 10^{-3}$ new features emerge. The calculations for negative β continue to remain near the $I_R^{(n=10)}(\beta)$ line. But, for positive β values, a fine resonance structure is encountered around $\beta \cong 1.7 \times 10^{-3}$ and a sharp increase in $I_R(\beta)$ is observed at $\beta \cong 2 \times 10^{-3}$, followed by a regular oscillation pattern which on the average increases according to a β^2 law. These structures have quantum-mechanical origins and can be explained in the following way.

Consider the quantum map (4.4), and, in particular, the operator W . It acts as an effective Hamiltonian, and it

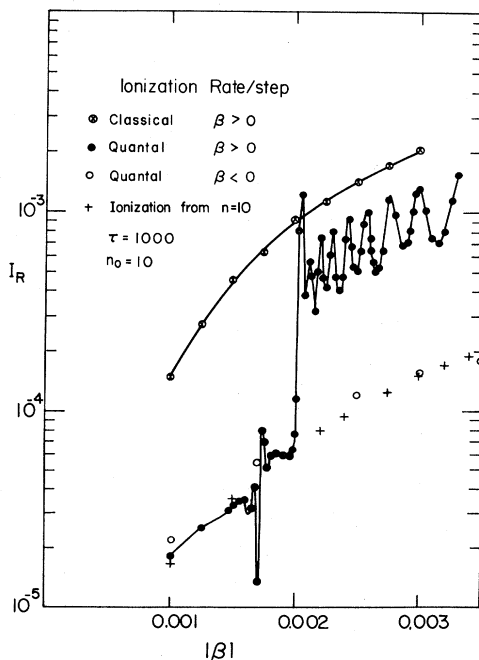


FIG. 9. Ionization rates calculated in various approaches for $\tau=1000$. Lines through the points are drawn to guide the eye.

can be expressed as a function of H_0 and V via the Hausdorff-Baker expansion.¹⁰ Neglecting the commutators in this expansion, we obtain a semiclassical expression for W :

$$W^{sc} = \tau \left[p^2 - \frac{2}{q} \right] - \beta q \quad (4.14)$$

and $p = i\partial/\partial q$. The eigenvectors of W determine the properties of the system. The effective potential term $-2\tau/q - \beta q$ changes its character when β changes its sign. When $\beta < 0$ the effective potential has only bound states, even for positive energies. The eigenfunctions corresponding to negative energies are not expected to change their character compared to the corresponding eigenfunctions of H_0 and therefore the properties which are due to localization will persist even when $|\beta|$ increases. This explains the observed regular behavior of $I_R(\beta)$ for $\beta < 0$.

For $\beta > 0$, the effective potential is not monotonic, reaching its maximum value of $-(8\tau\beta)^{1/2}$ at $q = (2\tau/\beta)^{1/2}$. All the eigenfunctions of W^{sc} are continuum states. The continuous part of the spectrum, which for H_0 was bounded by a threshold at $E=0$, is now extended to negative energies and the threshold shifts to $E = -(8\tau\beta)^{1/2}$. At lower energies resonance states with energies $E_n \cong -\tau/n^2$ dominate the spectrum. They are embedded in a continuum of states. The widths of the resonances decrease rapidly with decreasing n . It is therefore to be expected that the ionization rates will be strongly affected by the threshold and resonances mentioned above if $|\Psi_N\rangle$ has an appreciable overlap with a state $|n\rangle$ whose energy, $-\tau/n^2$, exceeds the threshold or accidentally overlaps with a resonance near threshold. The energy of the initial state ($n=10$) becomes equal to the threshold energy only at $\beta=0.0125$ which is far beyond the range of β investigated here. However, the state with $n=16$ is resonantly mixed with the state $n=10$ since $1000(1/10^2 - 1/16^2) \cong 0.189 \pmod{2\pi}$. The energy of the $n=16$ state becomes equal to the threshold energy at $\beta=0.00191$ and to the energy of the first bound resonance at $\beta=0.00171$. These two values are very close to the points where the sudden increase in $I_R(\beta)$ and the resonance structure occur in our results. The state $n=17$ fulfills the resonance condition to a somewhat lesser extent [$1000(1/10^2 - 1/17^2) \cong 0.257 \pmod{2\pi}$] and, because of the decreasing value of the matrix element to the higher- n state, its effect is unnoticed even at $\beta=0.00149$ which corresponds to $n=17$ at threshold. The origin of the oscillations which appear for $\beta > 0.002$ is not entirely clear to us. They reflect the interfering contributions of several n states to the ionization amplitude. We are certain, however, that they are not due to a numerical artifact.

The above discussion of the systems with $\tau=500$ and 1000 illustrates the sensitivity of the ionization rates to various details in the wave function. In this sense, the ionization rates can serve as a powerful probe to understand the quantum dynamics of the periodically kicked SSE.

C. Inclusion of continuum effects—higher order

The expression (4.11) can be shown to be the lowest-order term in a systematic expansion of the exact iteration of the quantum mapping. Let

$$U = e^{-iW},$$

$$P = \sum_{n=1}^{\infty} |n\rangle\langle n|, \quad Q = I - P = \int_0^{\infty} |\chi\rangle d\chi\langle\chi|,$$

$$U_{PP} = PUP, \quad U_{PQ} = PUQ, \quad \dots$$

The quantum mapping can be rewritten in the following way:

$$|P\Psi_{k+1}\rangle = U_{PP}|P\Psi_k\rangle + U_{PQ}|Q\Psi_k\rangle,$$

$$|Q\Psi_k\rangle = U_{QP}|P\Psi_{k-1}\rangle + U_{QQ}|Q\Psi_{k-1}\rangle$$

$$= \sum_{j=1}^k (U_{QQ})^{j-1} U_{QP}|P\Psi_{k-j}\rangle.$$

Hence,

$$|P\Psi_{k+1}\rangle = U_{PP}|P\Psi_k\rangle$$

$$+ U_{PQ} \sum_{j=1}^k (U_{QQ})^{j-1} U_{QP}|P\Psi_{k-j}\rangle. \quad (4.15)$$

In deriving (4.15) explicit use is made of the fact that $Q|\Psi_0\rangle = 0$. The mapping (4.4) is now expressed in terms of the P -space variables only, at the expense of introducing memory terms into the mapping, i.e., $|P\Psi_{k+1}\rangle$ is not a function of $|P\Psi_k\rangle$ only, but of all the previous $|P\Psi_{k-j}\rangle$, $j=1, 2, \dots, k$. The approximation used in Sec. IV B was obtained by neglecting *all* the memory terms in (4.15). In this section we shall investigate briefly the role of the term with $j=1$ and neglect the rest. In this approximation all terms which include U_{QQ} are neglected, in other words, continuum-continuum transitions are ignored.

The numerical evaluation of the matrix $U_{PQ}U_{QP}$ involves integrals of the type

$$\int_0^{\infty} d\chi \langle n | e^{-iV} | \chi \rangle e^{-i\pi(2\chi/\alpha)^2} \langle \chi | e^{-iV} | n' \rangle. \quad (4.16)$$

The matrix elements $\langle n | e^{-iV} | \chi \rangle$ were discussed in Sec. IV B and analytical expressions are given in the Appendix. The χ integration was performed numerically. The integrand is an oscillatory function, and in order to achieve sufficient accuracy in the result, intricate integration methods together with a fine integration grid had to be

applied. Because of the amount of computer time involved in these calculations, we were able to perform only a few sample runs.

With the matrix $U_{PQ}U_{QP}$ calculated, we could proceed with the modified quantum map. Comparing the results with the ones obtained from iterating (4.11) we find that in all the cases checked, the ionization rates as well as the moments of the energy distribution in the P space are altered by at most a few percent. This supports the validity of the approximation used in Sec. IV B for the range of variables of interest here.

V. SUMMARY

The main conclusion of the present work is that the classical stochasticity which manifests itself in the energy diffusion and ionization rates is suppressed by quantum effects. The quantum description is dominated by the localization property of the initial state in the quasienergy representation, and due to localization the energy distribution and the ionization rates reflect the properties of only a few coherently interfering states. We have also shown that the features observed in the ionization rates are sensitive to the detailed structure of the wave function. If one could measure them in actual experiment they would provide a very powerful probe to study the quantum-mechanical effects in this system.

There are two important problems which still await solution. (a) We have seen that the behavior of the periodically kicked SSE, as well as that of the periodically kicked rotor, is completely determined by one and the same mechanism—localization of the wave function in the quasienergy basis. Whether this is a general property, or whether one can set conditions under which delocalization occurs, remains an open question. (b) The comparison of the quantum and classical descriptions of the rotor and the SSE systems shows that in the long-time limit the quantum-mechanical description does not seem to approach the classical picture even when large ($n=10$) quantum numbers are involved. The reasons for this apparent disagreement begin to emerge from recent studies, although a semiclassical method which makes use of classical dynamics to approximate the quantum description is still lacking.

ACKNOWLEDGMENTS

We would like to thank Dr. S. Fishman, Dr. H. Schuster, Dr. D. Mukamel, and Dr. B. Schaub for very valuable discussions and suggestions. One of us (R.B.) acknowledges the receipt of a Minerva Student Award, which supported his stay at the Weizmann Institute when this work was done.

APPENDIX

In this Appendix we quote some results for integrals¹¹ which are required for the quantum-mechanical description of SSE.

1. Matrix elements of $V = -\frac{1}{2}\beta(\alpha x)$

We use the identity

$$xL_n^{(1)}(x) = (n+1)[L_{n+1}^{(1)}(x) - 2L_n^{(1)}(x) + L_{n-1}^{(1)}(x)] \quad (A1)$$

to rewrite

$$\begin{aligned}
 V_{nm} &= \frac{\beta}{2} \langle n | \alpha x | m \rangle \\
 &= \frac{\beta}{4} \frac{1}{\sqrt{nm}} \int_0^\infty dy \exp \left[-\frac{1}{2} \left[\frac{1}{n} + \frac{1}{m} \right] y \right] y [L_n^{(1)}(y/n) - 2L_{n-1}^{(1)}(y/n) + L_{n-2}^{(1)}(y/n)] \\
 &\quad \times [L_m^{(1)}(y/m) - 2L_{m-1}^{(1)}(y/m) + L_{m-2}^{(1)}(y/m)]
 \end{aligned} \tag{A2}$$

and define

$$\begin{aligned}
 I_{pq}^{(nm)} &= \frac{1}{4} \int_0^\infty \exp \left[-\frac{1}{2} \left[\frac{1}{n} + \frac{1}{m} \right] y \right] y L_p^{(1)}(y/n) L_q^{(1)}(y/m) dy \\
 &= 4^q \frac{(p+1)}{(nm)^q} \frac{\left[\frac{1}{m} - \frac{1}{n} \right]^{p-q}}{\left[\frac{1}{m} + \frac{1}{n} \right]^{p+q+2}} P_q^{(p-q; -p-q-2)}(s),
 \end{aligned}$$

where $P_\gamma^{(\nu, \mu)}(s)$ is the Jacobi polynomial and $s = \frac{1}{2}(n/m + m/n)$. The Jacobi polynomial can be easily evaluated and V_{nm} is expressed as a sum of nine integrals $I_{pq}^{(nm)}$ with $n \geq p \geq n-2$, $m \geq q \geq m-2$ as implied by Eq. (A2).

2. Matrix elements of e^{-iV} between bound states

Using the identity (A1) we transform

$$\begin{aligned}
 \langle n | e^{-iV} | m \rangle &= -\frac{n^2}{2(nm)^{5/2}} \int_0^\infty dy \exp \left[-\frac{1}{2} \left[\frac{1}{n} + \frac{1}{m} - i\beta \right] y \right] y \\
 &\quad \times L_{m-1}^{(1)}(y/m) [L_n^{(1)}(y/n) - 2L_{n-1}^{(1)}(y/n) + L_{n-2}^{(1)}(y/n)]
 \end{aligned} \tag{A3}$$

and define

$$\begin{aligned}
 J_{nm}^{(k)}(\beta) &= \int_0^\infty dy \exp \left[-\frac{1}{2} \left[\frac{1}{n} + \frac{1}{m} - i\beta \right] y \right] y L_{n+1-k}^{(1)}(y/n) L_{m-1}^{(1)}(y/m) \\
 &= 4^m \frac{(n+2-k)}{(nm)^{m-1}} \frac{\left[\frac{1}{m} - \frac{1}{n} - i\beta \right]^{n+2-m-k}}{\left[\frac{1}{m} + \frac{1}{n} - i\beta \right]^{n+2+m-k}} P_{m-1}^{(n+2-m-k; -n-2-m+k)}(s(\beta))
 \end{aligned}$$

with $s(\beta) = (mn/2)(1/m^2 + 1/n^2 + \beta^2)$, $k=1,2,3$, and $J^{(1)} = J^{(3)} = 0$ for $n=m$ as $\beta \rightarrow 0$. Hence

$$\langle n | e^{-iV} | m \rangle = -\frac{n^2}{2(nm)^{5/2}} [J_{nm}^{(1)}(\beta) - 2J_{nm}^{(2)}(\beta) + J_{nm}^{(3)}(\beta)]. \tag{A4}$$

3. Matrix elements of e^{-iV} between bound and continuum states

Using the identity (A1) and expressing the Laguerre polynomials and the Coulomb wave functions as confluent hypergeometric functions, the desired matrix element is expressed as a combination of three integrals of the kind

$$\begin{aligned}
 K_{mn}(\beta; \eta) &= \frac{1}{4} \int_0^\infty dt \exp \left[-\frac{1}{2}(1 - in/\eta - in\beta)t \right] {}_1F_1(-m, 2; t) {}_1F_1(1 - i\eta, 2; -i(n/\eta)t) \\
 &= \frac{(-1)^m}{m+1} \frac{1}{(1 - in\beta)^2 + (n/\eta)^2} \left[\frac{1 + in/\eta + in\beta}{1 - in/\eta - in\beta} \right]^m \\
 &\quad \times \left[\frac{1 + in/\eta - in\beta}{1 - in/\eta - in\beta} \right]^{i\eta} P_m^{(1; -(m+1+i\eta))} \left[1 - \frac{8in/\eta}{(1 + in/\eta)^2 + n^2\beta^2} \right],
 \end{aligned}$$

where

$$\eta = -\alpha/2\chi .$$

Thus

$$\langle n | e^{(1/2)i\beta(ax)} | \chi \rangle = \frac{n}{\eta} \left(\frac{2n}{\alpha} \right)^{1/2} \left(\frac{4\eta}{e^{2\pi\eta} - 1} \right)^{1/2} [(n+1)K_{nn}(\beta, n) - 2nK_{nn-1}(\beta, \eta) + (n-1)K_{nn-2}(\beta, \eta)] . \quad (\text{A5})$$

*Present address: Institut für Theoretische Physik, Technische Universität München, D-8046 Garching, Federal Republic of Germany.

¹G. M. Zaslavsky, Phys. Rep. 80, 157 (1981), and references cited therein.

²M. V. Berry, N. L. Balazs, M. Tabor, and A. Voros, Ann. Phys. (N.Y.) 122, 26 (1979).

³G. Casati, B. V. Chirikov, F. M. Izrailev, and J. Ford, in *Stochastic Behavior in Classical and Quantum Hamiltonian Systems*, edited by G. Casati and J. Ford, Vol. 83 of *Lecture Notes in Physics* (Springer, Berlin, 1979).

⁴T. Hogg and B. A. Huberman, Phys. Rev. Lett. 48, 711 (1982); Phys. Rev. A 28, 22 (1983).

⁵D. R. Grempel, S. Fishman, and A. E. Prange, Phys. Rev. Lett. 49, 509 (1982); Phys. Rev. A (to be published).

⁶R. V. Jensen, Phys. Rev. Lett. 49, 1365 (1982).

⁷C. C. Grimes, T. R. Brown, M. L. Burns, and C. L. Zipfel, Phys. Rev. B 13, 140 (1976).

⁸A summary of the quantum-mechanical treatment was reported in R. Blümel and U. Smilansky, Phys. Rev. Lett. 52, 137 (1984).

⁹J. G. Leopold and I. C. Percival, J. Phys. B 12, 709 (1979).

¹⁰R. Englman and P. Levi, J. Math. Phys. 4, 105 (1963).

¹¹I. S. Gradshteyn and I. M. Ryzhik, *Table of Integrals, Series and Products* (Academic, New York and London, 1965).